Design and validation of a high DOF origami inspired soft actuated assistive exoskeleton arm and spine

Article

Accepted Version

Design and Validation of a High DOF Origami Inspired Soft Actuated Assistive Exoskeleton Arm and Spine

Daniel George, Sadao Kawamura, Ying Zheng, and Yoshikatsu Hayashi,

Corresponding author: Yoshikatsu Hayashi
Email: y.hayashi@reading.ac.uk
Address: School of Biomedical Sciences and Biomedical Engineering, University of Reading, Reading, Berkshire, UK

***Abstract*—This research presents the design, development, and validation of a high degree of freedom (DOF) exoskeleton actuated by origami-inspired soft inflatable modules. The objective was to create reliable soft actuators to provide safe and compliant movement assistance. Utilising lightweight 3D printing materials and origami-inspired soft flexible modules, the developed exoskeleton offers seven DOF to assist reaching motion of the upper limb. A passive rubber joint was incorporated for gravity compensation of the upper limb with elastic stability. The integrated exoskeleton consists of collapsible soft actuators made from polyethylene tubing, an ultra-lightweight structure with seven DOF, and real-time feedback through electronic goniometers.**

The validation included comprehensive testing of the soft actuators, and evaluating speed and accuracy. Torque measurements of the single module reached up to 4.46 Nm. A participant experiment in reaching motion demonstrated relatively slow but accurate movement, showcasing the effectiveness in assisting passive motion. This research successfully integrates soft actuators with a high DOF exoskeleton, highlighting its potential for providing movement assistance in various applications in future.

***Index Terms*—Exoskeleton, Soft Robotics, Assistive Device, Medical Robot, Human-Robot Interaction.**

I. Introduction

MUSCLE weakness manifests as a common symptom associated with diverse medical conditions. For instance, individuals who have experienced a stroke may encounter a partial loss of neurological connectivity with their muscles [1], [2]. Additionally, muscle weakness can result from physical trauma, insufficient muscle engagement, or as a secondary effect of other underlying issues. The management of these conditions typically involves physical therapy interventions aimed at restoring neural pathways through repetitive movements or enhancing muscle strength through resistance training [3].

Therapeutic interventions often involve the utilisation of assistive tools, such as inflatable balls that patients can squeeze to enhance muscle strength or supportive braces to aid in movement [4]. However, these technologies often lack customisation options tailored to individual patients. Furthermore, advanced technologies with intelligent features tend to be costly, limiting their accessibility to a broader population. Consequently, there exists a compelling need for affordable and reliable solutions that can be tailored to meet the unique needs of each patient [3].

The current scarcity of medical personnel, particularly in the UK, has underscored the need for technological advancements to alleviate their workload. Moreover, the integration of more sophisticated medical technology would empower patients by enhancing their personal freedom and individuality throughout the treatment process. In this context, exoskeletons have emerged as a promising medical device to address the aforementioned challenges [5], [6].

Exoskeletons are wearable devices designed to provide physical assistance, augmenting the user's strength, stamina, or movement precision [7]. However, conventional exoskeletons often suffer from bulkiness and are composed of heavy metal components with attached motors to actively assist the user's movements [8], [9]. The significant inertia associated with these metal-based exoskeletons hampers natural user motion and necessitates complex impedance control strategies [10]. Consequently, there is a pressing need for more compliant and safer robotic technologies in the development of assistive devices within the medical domain. These technologies should possess lower inertia and inherent impedance characteristics derived from the materials themselves, obviating the need for intricate impedance control mechanisms to generate desired forces.

Ongoing research efforts focused on developing more user-compliant exoskeletons have explored various approaches to reduce weight and enhance functionality. One approach involves the relocation of servo motors away from the joints and use a pulley system, enabling the use of cables to transmit forces and facilitate movement [11]. Another approach entails replacing traditional motors with air pumps and utilising inflation-style actuators like the 'McKibben' system, which aims to replicate the natural actuation of muscles [12]. This substitution can significantly decrease the size and weight of the exoskeleton while maintaining the required actuation capabilities. Additionally, current research explores softer actuation methods by employing silicone inflatables as a substitute for electric motors [13].

Recent advancements in exoskeleton research have led to the emergence of "exosuits" that offer enhanced user compliance and functionality [14]. These exosuits, designed to resemble clothing rather than rigid frames, incorporate the use of pulley systems for actuation. However, the absence of a rigid frame in exosuits poses challenges related to stability and increased

susceptibility to errors. An important objective in exoskeleton development is to achieve a balance between providing a high degree of freedom (DOF), comparable to that of robust metal exoskeletons, and ensuring lightweight characteristics similar to exosuits.

This study focuses on the development of an ultra-lightweight exoskeleton integrated with soft and lightweight modules. By leveraging the advantages of both lightweight actuators and exoskeleton components, we aim to create a wearable system that offers enhanced user comfort and minimal discomfort during use.

The proposed device utilises polylactic acid (PLA+) as the primary material for the exoskeleton structure. This choice of material significantly reduces the overall weight of the device, reaching a mere 572 g. In comparison, conventional metal designs can weigh over 11 kg [15], with some developments even exceeding 180 kg. By employing PLA+, we achieve a lightweight frame that ensures stable movement for the user.

Unlike traditional exoskeletons that rely on static attachments, which restrict the user's mobility and impede actions such as standing up, sitting down, leaning, and moving freely within a given area, our proposed device offers enhanced freedom of movement. To enhance wearer flexibility, we propose a user-carried design where the control box is separated from the main body of the exoskeleton. This separation allows for improved mobility and greater user autonomy during operation.

Soft actuators offer promising applications in robotic systems that interact with delicate objects or individuals, making them particularly well-suited for medical environments [16]. One notable advantage of the soft actuators in this study is their operation at pressures near atmospheric levels [17]. While rigid pneumatic actuators can operate effectively at various pressure levels, including near atmospheric, the soft polyethylene actuators exhibit lower pressure requirements due to the lightweight and flexible material. Moreover, the reduced reliance on electrical components in the soft actuators contributes to a safer environment by minimising potential electromagnetic interference with nearby medical equipment or patient implants.

Soft actuators possess a distinctive strength derived from their inherent functional flexibility. Unlike 'hard' actuators such as servo motors, which are limited to a single DOF, soft actuators offer the potential for multiple DOFs. Hard motors maintain the highest level of stiffness possible whilst working to maximise work efficiency, regulating stiffness in such systems necessitates intricate supplementary mechanisms [10]. In contrast, soft actuators can be less stable but demonstrate a remarkable capability to adjust their stiffness based on specific requirements by leveraging the inherent properties of the material. This ability to control the generated force through impedance control is a distinguishing feature of soft actuators.

By precisely regulating the internal air pressure of the inflatable modules, the required force to actuate the soft actuators, and consequently the connected user, can be adjusted. This inherent controllability enables fine-tuning the level of support provided to the user. This aspect finds direct relevance in the realm of physical therapy, where the ability to customise resistance according to individual needs and progressive strength development is crucial [18]. The actuators can amplify the movement along the desired trajectory and reduce the effort exerted by the user. As the user's strength improves, the resistance of the exoskeleton can be incrementally increased, thereby diminishing the level of assistance or even introducing a negative force to further challenge and engage the targeted muscles [19].

In contrast to electric motors, which demand rapid and precise control to synchronise the motor assistance with the unpredictable motion of users [10], soft actuation presents an alternative approach. The inherent challenge with heavy robotic systems lies in the coordination of motor acceleration to match the impedance characteristics (including inertia, viscosity, and elasticity) of the system. This impedance control, implemented through motor acceleration, tends to be noisy by nature. Consequently, there exists a pressing need to transfer the burden of impedance control from the motor to the material itself [20]. Soft modules can assume a significant role in actuation by generating torque for the joints and imparting appropriate viscoelastic properties to facilitate joint rotation [21]. By leveraging the inherent characteristics of the soft material, this approach offers the potential to achieve more seamless and efficient actuation while minimising the complexities associated with traditional motor-based control systems [22].

Taking inspiration from the Japanese art of origami, our study explores the potential of achieving a wide range of actuation capabilities using thin, paper-like materials with a thickness of less than 1mm [23]. The application of origami principles has demonstrated remarkable versatility across various fields, including satellite deployment to optimise space utilisation in rockets [24], sun-tracking solar panels for enhanced energy efficiency [25], and compact robotic systems [26]. In the realm of soft robotics, the incorporation of origami concepts has recently garnered attention for "soft touch" applications like grippers [27], which prove valuable in delicate handling tasks such as fruit manipulation. By utilising origami-inspired folding structures, our soft actuators offer the advantage of space-saving designs while maintaining minimal volume changes to generate targeted forces in desired directions.

The study by Chang et al. [28] demonstrates the need for a high range of motion to match the DOF that is produced by the human body for effective rehabilitation. This high range of motion can only come from rigid exoskeletons that is anatomically aligned to the user's body. The soft modules are able to accommodate the high range of motion needs of the exoskeleton as they virtually have an infinite DOF due to the soft body. In the study by Victoria et al. [17] the hybrid system is demonstrated to be ideal for assistive application.

In summary, the current research gap lies in developing a safe and functional exoskeleton that utilises reliable soft actuation to assist user movement, while achieving paper-thin compactness to save space which is not typically observed in silicone or soft pneumatic actuators.

It is essential to incorporate a high number of degrees of freedom in the device to facilitate the rehabilitation process

and enable users to achieve a full range of motion in their upper limbs [28], including novel supination and pronation movements. This objective necessitates overcoming the inherent bulkiness often associated with traditional metal designs and silicon base modules.

Some notable examples of similar exoskeletons are as follows: In a study by Kousidou et al. [29], a device employing soft pneumatic actuators in combination with a rigid exoskeleton was developed to provide assistance for 7 DOF in the upper limb, specifically targeting rehabilitation applications. While this design is relatively lightweight and compact, it allows motion over only 75% of the normal operating volume. Another 7-DOF assistive device [30] utilises a tendon cable transmission and features a circular joint to facilitate supination and pronation movements. However, the complexity and bulkiness of this design are evident. Fully soft exoskeletons, on the other hand, face limitations in movement due to the absence of rigid structures to operate from, as highlighted in a study by Ma et al. [31].

The primary objective of our study is to evaluate the design and functionality of the soft actuators, both individually and in conjunction with the high DOF exoskeleton, using a healthy-bodied user to test the assistive functionality in reaching motion. This research serves as a crucial step towards adapting the technology for clinical settings, where it can benefit individuals with vulnerable bodies. The main challenges encountered in this endeavour include replicating the movement of internal joints externally. Additionally, a key focus is to develop robust soft actuators capable of withstanding high forces without failure. Addressing these challenges is vital for advancing the feasibility and efficacy of the device in real-world applications.

These considerations lead to the design specifications for the 3D printed exoskeleton actuated by the soft modules are as follows:

- Mechanical Structure: The 3D printed exoskeleton should be designed to enable high degrees of freedom for upper limb motion within a three-dimensional workspace.
- Origami Structure: The soft actuators should be folded in an origami-like structure to facilitate the generation of torque and ensure appropriate embedded compliance.
- Passive Gravity Compensation: The exoskeleton should incorporate passive gravity compensation to assist in lifting the weight of the entire arm, reducing the strain on the user
- Trajectory Guidance: The exoskeleton should provide accurate guidance for the trajectory of the user's arm when reaching for objects, ensuring precise and controlled movements.
- Attachment Capability: The exoskeleton should be attachable to a body harness, serving to support the weight of both the exoskeleton and the user's arm. This attachment point will also act as an anchor, enabling smooth operation and stability.

The subsequent sections of this paper provide detailed information on the construction of the exoskeleton and the fabrication of the soft actuators. The individual performance of the actuators was assessed, considering factors such as torque, inflation speed, and the resulting angles achieved. The integrated system's validation was conducted by assisting the user in reaching targets within the three-dimensional workspace.

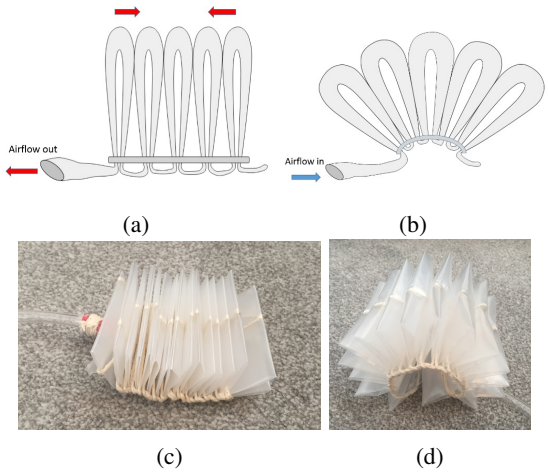

Fig. 1: (a) The diagram depicts the deflated state of the actuator. When the actuator is inflated, the loops push into neighboring loops, causing the actuator to expand in the desired direction. The expansion is governed by the constraint at the bottom, as shown in diagram (b). (c) The deflated actuator designed for rotation joints has a width of 7.5 cm. The constraint, which determines the circumference of the actuator, is matched to the circumference of an arm. When inflated, the actuator can expand around the outside of an arm in an arch shape. (d) After inflation, the actuator exhibits a curved shape, which can reach a maximum curvature of up to 360 degrees.

II. Material and Methods

A. Soft Actuators

The selection of the material for the soft actuators was based on their desired characteristics of flexibility and durability. To assess various materials, comparisons were made using stiffness, strength, and density data from materials and process charts by Mike Ashby [32]. The chosen material needed to have a Young's modulus below 10 GPa to ensure flexibility, a density lower than 8000 kg/m^3, and a strength higher than 3 MPa to prevent tearing. This narrowed down the options to elastomers and polymers.

In this study, the soft actuators were fabricated using polyethylene tubing and string. The string was twisted into a double helix and inserted into the polyethylene tube, ensuring that there were no kinked folds to allow unrestricted airflow. One end of the actuator was heat-sealed, while the other end had an intake tube inserted to facilitate air pumping. The tube was then folded into a zigzag pattern, and the folds were secured using string along one side, as depicted in Fig. 1.

The actuators were configured to exhibit different movements based on the level of constraint applied to the loops using string. For instance, when the loops were tightly constrained along one side, inflation resulted in the formation of an arch shape, as depicted in Fig. 1b and Fig. 1d.

Two types of actuators, namely hinge-style actuators and rotation-style actuators, were employed in conjunction with

the exoskeleton. Each actuator consisted of 13 loops, with each loop measuring 7 cm in length as seen in Fig. 1c and Fig. 1d. While these actuators shared a similar structural composition, they differed in terms of the degree of constraint along one side. Hinge-style actuators featured a higher level of constraint, leading to a tighter curvature upon inflation. Consequently, these actuators were well-suited for facilitating precise movements in hinge joints such as the elbow or shoulder.

Conversely, rotation-style actuators were characterised by a relatively looser constraint along one side. This design allowed for a more gradual and wider curvature, enabling smooth rotation around the circumference of the arm. As a result, rotation-style actuators proved advantageous for facilitating movements in rotation joints that control the supination and pronation movements.

By manipulating the level of constraint, the actuators were tailored to accommodate various joint types and ensure accurate targeting during user-assisted movements as depicted in Fig. 3.

B. Exoskeleton

In the upper limb exoskeleton illustrated in Fig. 2a, three exoskeleton joints represent the corresponding joints in the human arm. The first type is the single hinge joints with 1 DOF, situated at the wrist and elbow to facilitate flexion and extension movements. An example of an elbow hinge joint was demonstrated in Fig. 2b, located at the connection between P1 and P2.

The second type consists of rotation joints responsible for generating supination and pronation motions, these are labeled as 'Rotation 1 (Forearm)' and 'Rotation 2 (Shoulder)' in Fig. 2a. These joints are positioned in the forearm and above the elbow. Fig. 2c displays an X-ray of the upper arm rotation joint.

Additionally, a ball and socket joint is present at the shoulder. In the exoskeleton, this joint is divided into two interconnected joints. The first joint, labeled as 'shoulder' in Fig. 2a, corresponds to a hinge joint configuration.

The second joint, referred to as the gravity compensation joint, serves the purpose of connecting the shoulder and the elbow. Elastic strips made from rubber are utilised in this joint and can be easily replaced to avoid deterioration. The elastic strips play a crucial role in maintaining the arm's elevation and alignment with the workspace. Unlike the other active joints, this joint operates passively. The connection points for these elastic strips are labeled as 'GP1' and 'GP2' in Fig. 2b. This design approach serves two primary purposes: first, it alleviates the weight of the shoulder joint, which involves lifting the entire arm against gravity — a challenging task for a soft actuator. Second, by reducing the burden on the shoulder joint, the system can prioritise the accuracy of target reaching.

To wear the device, the user is required to position their arm through the cylindrical opening, allowing for subsequent connection to the back region. While straps are provided for user attachment, they were found to be generally unnecessary. Given the aim to replicate the internal joints and replicate their

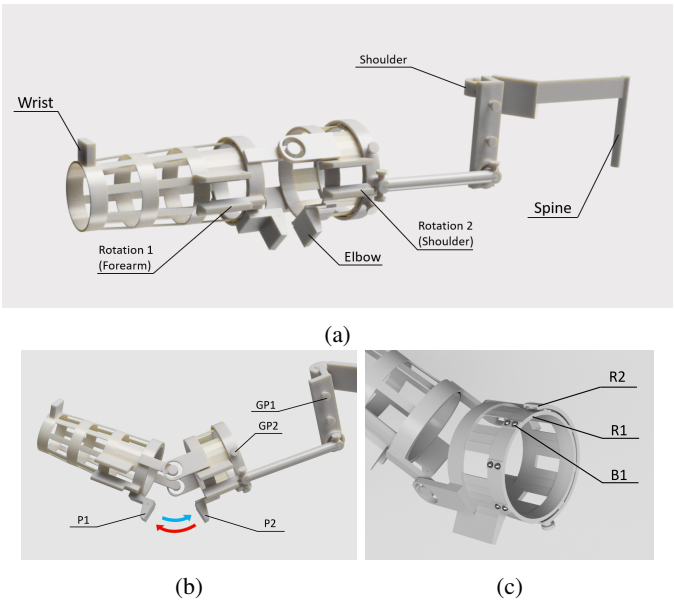

Fig. 2: Structure of the exoskeleton. (a) The comprehensive CAD model illustrating the complete exoskeleton design.(b) The exoskeleton arm demonstrates flexion at the elbow joint, with P1 and P2 representing the platforms where the actuators are affixed. The inflation of the actuator induces the bending of the lower arm in relation to the upper arm, as indicated by the directional arrows. GP1 and GP2 serve as attachment points for elastic strips employed in gravity compensation, maintaining the arm in an elevated position. The length of the elastic strips determines the arm's angle relative to the shoulder, while their elasticity ensures comfort and flexibility during tasks.(c) The rotation mechanism: R1 and R2 denote the inner and outer rings, respectively, while B1 corresponds to the ball bearings resting within the grooves of R1. R2 is connected to the upper arm, and R1 is linked to the lower arm. As the platforms connected to their respective rings are pushed apart by the actuator, R1 undergoes rotation, facilitating the rotational movement of the lower arm.

external functionality, it becomes necessary to tailor the size of the device to match the specific dimensions of the wearer. Consequently, The size of the device is currently made to be aligned with anatomical specification of the user.

Fig. 3 illustrates the exoskeleton worn by a user, showcasing the integrated actuators, harness, and spine. The one objective is to provide the user with a means of carrying the device, weighing 1.8 kg (excluding the separately connected control system via air tubes), while enabling mobility and various body movements such as leaning, standing up/sitting down, and navigating the surroundings.

In the depicted image, the user is observed wearing a harness, which serves as a foundational element for the exoskeleton system. Complementing the harness is a 3D-printed spine that plays a crucial role in connecting and elevating the exoskeleton arm. The spine, resembling the natural structure of vertebrae, consists of interlocking segments stacked atop each other. Each segment features three openings at its left,

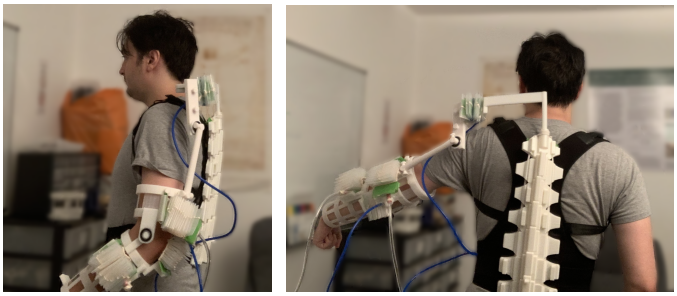

(a) (b)

Fig. 3: The printed exoskeleton with soft actuators is worn by a user. (a) The arm is at rest. (b) The arm extended.

right, and center, through which elastic cords pass and connect neighboring segments in series (see Fig. 4).

By incorporating elastic cords within the spine structure, a counterforce is generated to resist the user's back incline, effectively guiding them into an upright vertical position. This corrective mechanism helps maintain the user's natural standing or sitting posture by keeping the trunk of the body vertical. Moreover, the elastic cords facilitate the distribution of the device's weight along the user's back, contributing to enhanced stability and support. The design of the spine exemplifies the principle of tensegrity, where isolated components are under continuous tension, resulting in a stable and resilient structure [33]. In this case, tensegrity is employed to provide support to the user and the exoskeleton system.

Adjustability is a key component of the exoskeleton spine, as finding the optimal level of elasticity for the user can be challenging. Striking the right balance between providing adequate support and maintaining a comfortable range of motion is crucial.

During the experiment, the elastic properties of the exoskeleton spine were regulated to enable the user to achieve a controlled forward lean of approximately 45 degrees from the initial seated upright position. This inclination was distributed across eight individual segments of the exoskeleton spine, each equipped with adjustable elastic elements. By adjusting the tension of these elastic components the user is able to lean comfortably and securely while maintaining stability and support provided by the exoskeleton.

C. Control

A single pump (12 V, 5 L/min, inflation 120 kPa, deflation -65 kPa) was employed to inflate and deflate all actuators connected in series. To regulate the airflow and determine which actuators should be inflated or deflated, solenoid valves were utilised. These valves provide precise control over the distribution of air among the actuators.

The control box, weighing 2.2 kg, was independent of the worn exoskeleton and was connected to it through 8 mm air tubes and wire from the sensors. The control box operates on DC voltage and incorporates a microcontroller, specifically an Arduino Uno, to manage the overall control system. Additionally, 11.43 cm flex sensors were employed as

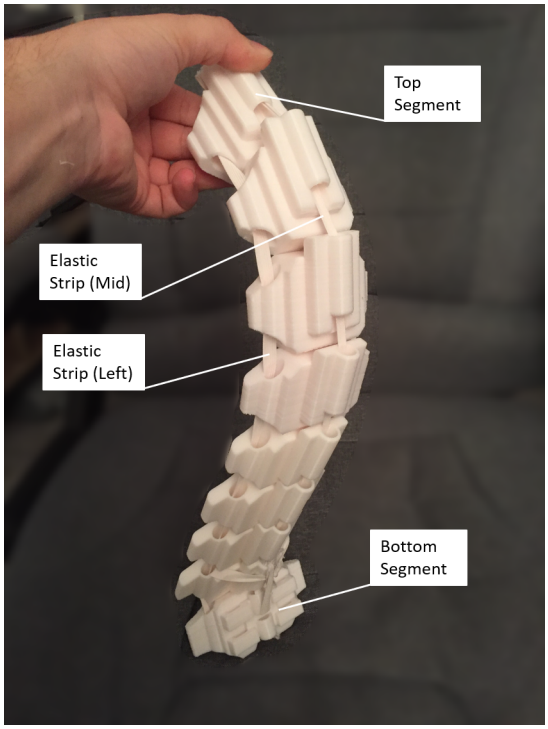

Fig. 4: 3D printed model of the spine segments connected together via elastic strips.

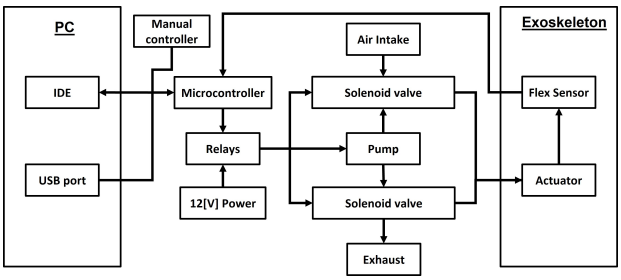

Fig. 5: The control diagram shows the connection between the components.

the primary sensing element within the exoskeleton system. Fig. 5 shows the connectivity between the components.

It is important to note that the control box may generate an operating noise level of approximately 60 dB within a one-metre range. Careful consideration should be given to noise management strategies to minimise any potential disturbances or discomfort to the user.

The movement execution in the exoskeleton system was based on a predefined movement plan, which included predetermined trajectories for the upper limb. These target distances are then translated into specific activation times for the pumps and solenoid valves, enabling the inflation and actuation of the corresponding joints. The correlation between the activation time of the pump and the resulting angular position of the joint is established through individual actuator tests, as illustrated in Fig. 10.

To measure the angular position of each joint, a voltage divider circuit is constructed, incorporating a flexible sensor known as an electronic goniometer. The flex sensors exhibit a

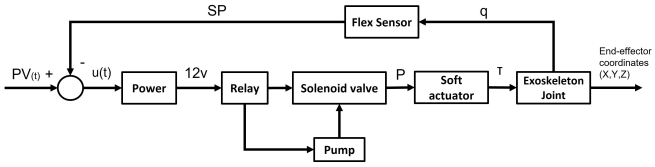

Fig. 6: The block diagram represents how the proportional control feedback is passed through the system.

change in internal resistance corresponding to their inclination, allowing for the conversion of this resistance change into angular degrees. Each joint is equipped with one sensor, which is calibrated to the specific shape and range of motion of that joint.

Proportional control was employed using the sensor readings to control the joints to the target values. If there is a discrepancy between the target angle and the sensor reading, the time taken to inflate the actuator to reach the target angle is modified to accommodate the discrepancy.

In cases where a consistent error persists, the proportional control gain K_p may be modified to enhance precision or an offset can be applied to the joint angle input $PV(t)$ to compensate for any systematic deviations. However, the control gain K_p and the joint angle input $PV(t)$ did not require modification during the experiment. These control mechanisms ensure accurate alignment of the joint positions with the intended target angles, facilitating precise movement execution within the exoskeleton system.

The below equation gives the calculation for an offset amount to correct the joint angle:

$$u(t) = K_p e(t) \tag{1}$$

where $u(t)$ represents the pump offset timing, which determines the duration for which the pump should be activated or deactivated when controlling the actuators. $e(t)$ is the position error calculated as the difference between the setpoint SP and the current sensor reading $PV(t)$. The setpoint represents the desired position of the joint, and $PV(t)$ represents the target angle. K_p is the proportional gain, which is a tuning parameter that determines the strength of the control action. It determines the magnitude of the pump offset timing adjustment based on the position error.

To establish the target angles $PV(t)$, the exoskeleton is positioned into the target position, and sensor values are recorded. Subsequently, the later experiments depicted in Fig. 10 compare actuator Angle vs. Time and are utilised to determine the optimal duration for which the pump should remain active during actuator inflation, in order to achieve the desired angles. The joint angles throughout are input into the DH-parameters to determine the end-effector coordinates.

The proportional control approach provides a way to continuously correct the joint position based on feedback from the sensors. By adjusting the pump timing in proportion to the position error, the system aims to minimise the deviation and achieve accurate control of the joint movement.

For a visual representation of the signal flow within the network, refer to the block diagram presented in Fig. 6. By following the feedback loop depicted in the block diagram, the control system adjusts the pump offset timing based on the position error sensed by the flex sensors. This closed-loop control mechanism enables precise control of joint movement, ensuring accurate operation of the exoskeleton.

D. Experiment Setup

The experimental methods consisted of three main experiments.

In the first experiment, the angle of the actuators during inflation was measured against time. This test was conducted both with the actuators alone and when connected to an exoskeleton joint to investigate the influence of the exoskeleton mass on the accuracy of inflation. The experiment was repeated 40 times to ensure statistical significance.

The second experiment focused on measuring the torque and force of the actuators in different settings. The first setting involved changing the angle of the hinge joint from 20 degrees up to 100 degrees to examine the torque variation during inflation. The second setting involved a wide-angle arc, and the final setting involved linear inflation to measure the maximum force in Newtons in a single direction. The setup for these experiments is depicted in Fig. 7.

The third experiment required the user to wear the fully integrated device and maintain a relaxed state, without requiring any voluntary movement. Meanwhile, the exoskeleton assisted in reaching three targets placed to provide representative movement to each joint in reaching targets in 3-dimensional space. The predetermined trajectory was followed, and sensor error detection accounted for minor spontaneous movements and forces exhibited by the participant.

To obtain the target angles, the exoskeleton arm is initially positioned in the target configuration, and angle data is recorded from the sensors. This process is can be carried out by a physical therapist who determines the most suitable movements for the user. Subsequently, the user performs the repeated motions involving all joints to condition the joint motion and establish consistent movement patterns.

When the user reaches for a target, the movement sequence begins with the inflation of the first actuator located at the shoulder. Subsequently, the next actuator in the series, moving down the arm towards the wrist, is inflated and this process continues until the last actuator at the wrist. The inflation cycle then restarts from the shoulder, repeating the sequence until all actuators have reached their target angle. There are two cycles for each task reaching experiment and the movement of each joint is split between these two cycles. The incremental inflation approach serves two purposes. Firstly, it facilitates a more direct trajectory of the end-effector towards the target, enhancing precision and accuracy. Secondly, it proves beneficial in a clinical setting, where the focus is on each individual joint and the their is a need for slow and controlled movements.

The user's hand had a rotational capability of 90 degrees at the forearm, just below the elbow, allowing for wrist rotation. Additionally, the upper arm had a 90-degree rotation, enabling the hand to face either up or down relative to the table. In this experiment, the user was only required to touch the targets.

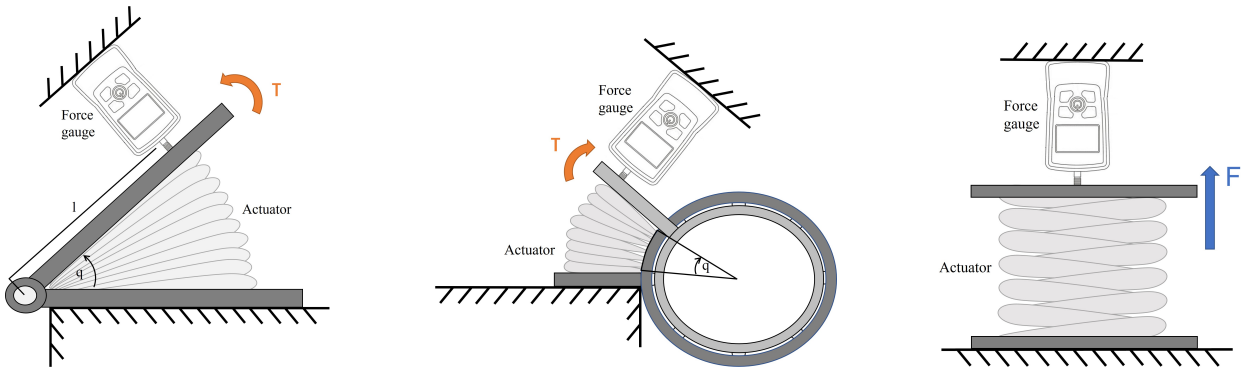

(a) (b) (c)

Fig. 7: (a) illustrates the force measurements for the hinge actuator with varying angles (q) at an axis of rotation distance of 0.12 m (l). The actuator was subjected to different angle positions, ranging from 20 degrees up to 100 degrees. (b) showcases the torque measurement set-up for the wide arc rotation. (c) presents the force measurements obtained during linear force inflation. The actuator was inflated linearly to evaluate the maximum force it could exert in a single direction.

To reach each target, five active actuators, one passive gravity compensation joint (the shoulder), and one joint without actuators (the spine) were utilised. The kinematics were pre-calculated to determine the target values of the joint angles. The trajectory of the user's hand, considered the end-effector, was plotted using a Cartesian coordinate system originating at the base of the shoulder (0, 0, 0). Flex sensors attached to the joints provided measurements in centimetres for accurate positioning.

The participant in this study was a healthy 30-year-old male with a height of 183 cm and an arms length of 72 cm, measured from the tip of the fingers on the left hand to the left shoulder. The participant maintained an upright sitting position on a chair in front of the table. The workspace and user setup are illustrated in Fig. 8. Informed consent was obtained from the participant for the conduction of this experiment.

To map the joint movements in relation to the targets, the exoskeleton is provided with coordinate frames. The base of the shoulder is defined at position (0, 0, 0) on the X, Y, and Z axes, respectively:

- The X-axis represents the medial and lateral rotation movement of the arm across the body, with 0 cm corresponding to a fully extended forward position in line with the body. Lateral movement from the user's perspective is denoted as negative movement notation, while medial movement across the body is considered the positive notation.
- The Y-axis corresponds to the elevation and depression movement of the arm. When the arm is fully extended forward perpendicular to the user's upright position, the Y-axis is at 0 cm, elevating the arm is considered positive movement notation and depressing the arm is the negative notation. Gravity compensation is applied from the shoulder to the elbow, maintaining the arm level with the working environment. The Y-axis is set at -22 cm.
- The Z-axis represents the abduction and adduction extensions relative to the user's body. The length of the arm from the shoulder to the wrist, when fully extended, is 57 cm. Abduction is the positive movement notation and adduction is the negative notation. The initial position of the end-effector is (0, -22, 57). The user is seated, and the target objects are placed on the table in front of them.

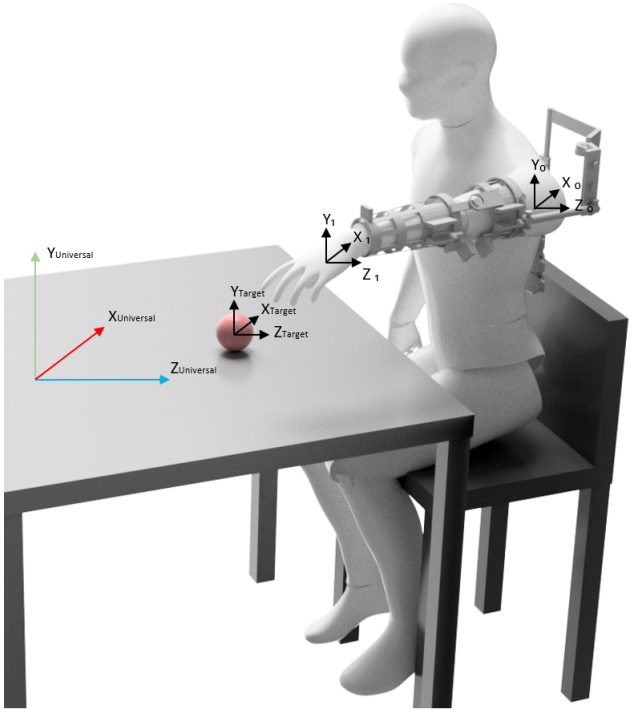

Fig. 8: Experimental setup and initial position with the user seated at a table and reaching for targets. The coordinates (X_0, Y_0, Z_0) represent the shoulder position, (X_1, Y_1, Z_1) denotes the location of the hand or end-effector, (X_T, Y_T, Z_T) indicates the position of the target on the table, and $(X_{Uni}, Y_{Uni}, Z_{Uni})$ refers to the universal coordinate system.

The target positions that the user is reaching for are as follows:

- The position of the first target object is (12, -26, 45). The distance from the starting position of the end-effector to this target object position is given by (12, -4, -12).

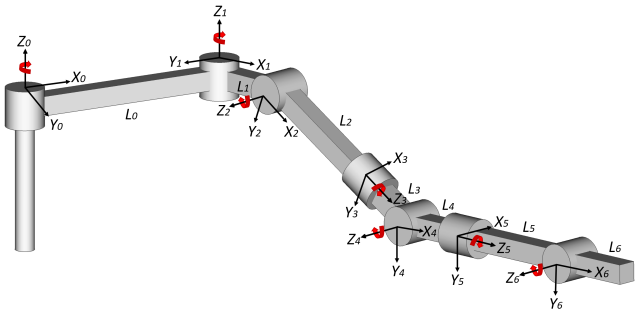

Fig. 9: Denavit-Hartenberg joint model of the human and exoskeleton arm. Each DOF is depicted as a cylinder rotating about its Z-axis, while its X-axis extends forward from the base towards the end-effector.

Link(*n*)	$\boldsymbol{\alpha}$	***d***	***R***	**Angle** θ
1	90°	0	L_1	θ_1
2	90°	0	0	θ_2
3	-90°	L_2 + L_3	0	θ_3
4	90°	0	0	θ_4
5	-90°	L_4 + L_5	0	θ_5
6	0°	0	L_6	θ_6

TABLE I: Denavit-Hartenberg parameters

- The position of the second target object is (30, -26, 20). The distance from the starting position of the end-effector to this target object position is given by (30, -4, -37).
- The position of the third target object is (20, -26, 30). The distance from the starting position of the end-effector to this target object position is given by (20, -4, -27).

E. Denavit-Hartenberg Parameters

Denavit-Hartenberg notations are used to find the forward kinematics of the 3D printed exoskeleton in Fig. 9.

Table I presents the Denavit-Hartenberg parameters used to describe the kinematic properties of the device. These parameters include α, which represents the angle about the common normal from the previous Z-axis to the new Z-axis. The offset along the previous Z-axis to the common normal is denoted by d, and R corresponds to the length of the common normal. Additionally, θ signifies the angle about the previous Z-axis from the old X-axis to the new X-axis. The lengths of the links are provided in Table II and denoted as L.

Each homogeneous transformation in the Denavit-Hartenberg method is typically represented as a product of four basic transformations. These transformations consist of a rotation about the X-axis, a rotation about the Z-axis, a translation along the X-axis, and a translation along the Z-axis.

$\boldsymbol{L_1}$**(mm)**	$\boldsymbol{L_2}$**(mm)**	$\boldsymbol{L_3}$**(mm)**	$\boldsymbol{L_4}$**(mm)**	$\boldsymbol{L_5}$**(mm)**	$\boldsymbol{L_6}$**(mm)**
100	200	80	80	80	40

TABLE II: Length of the exoskeleton links

$$^{n-1}T_n = D_{zn-1,dn}\, R_{zn-1,\theta n}\, D_{xn-1,Rn}\, R_{xn-1,\alpha n} \quad (2)$$

where

$$D_{zn-1,dn} = \begin{bmatrix} 1 & 0 & 0 & 0 \\ 0 & 1 & 0 & 0 \\ 0 & 0 & 1 & d_n \\ 0 & 0 & 0 & 1 \end{bmatrix} \quad (3)$$

$$R_{zn-1,\theta n} = \begin{bmatrix} c(\theta_n) & -s(\theta_n) & 0 & 0 \\ s(\theta_n) & c(\theta_n) & 0 & 0 \\ 0 & 0 & 1 & 0 \\ 0 & 0 & 0 & 1 \end{bmatrix} \quad (4)$$

$$D_{xn-1,Rn} = \begin{bmatrix} 1 & 0 & 0 & R_n \\ 0 & 1 & 0 & 0 \\ 0 & 0 & 1 & 0 \\ 0 & 0 & 0 & 1 \end{bmatrix} \quad (5)$$

$$R_{xn-1,\alpha n} = \begin{bmatrix} 1 & 0 & 0 & 0 \\ 0 & c(\alpha_n) & s(\alpha_n) & 0 \\ 0 & s(\alpha_n) & c(\alpha_n) & 0 \\ 0 & 0 & 0 & 1 \end{bmatrix} \quad (6)$$

$$^{n-1}T_n = \begin{bmatrix} c(\theta_n) & -s(\theta_n)C(\alpha_n) & s(\theta_n)s(\alpha_n) & R_n c(\alpha_n) \\ s(\theta_n) & c(\theta_n)c(\alpha_n) & -c(\theta_n)s(\alpha_n) & R_n s(\theta_n) \\ 0 & s(\alpha_n) & c(\alpha_n) & d_n \\ 0 & 0 & 0 & 1 \end{bmatrix} \quad (7)$$

where the transformation matrix $^{n-1}T_n$ represents the transformation from coordinate frame n to n-1. The variables $C(\theta)$ and $S(\theta)$ denote the cosine and sine of the angle θ, respectively. The parameters R_n and d_n are provided in Table I, which contains the specific values for each joint in the Denavit-Hartenberg model.

III. Results

A. Actuator Angle over Time measurements

The performance of the actuators was evaluated individually by subjecting both the hinge-style and rotational types to inflation and deflation tests. Initially, these tests were conducted in isolation, and subsequently, the actuators were integrated with the joints of the exoskeleton. To quantify the extent of movement, an internal flex sensor was utilised to measure the angular displacement in degrees. This measurement was then correlated with the inflation time. The resulting data, illustrating the average angle versus time profiles for the actuators, is graphically depicted in Fig. 10.

Fig. 10a and 10b depict the angular response of the isolated, inflated actuators prior to their connection with any joints. The observed results exhibit a degree of unpredictability.

In contrast, Fig. 10c and 10d display the angles of the actuators connected to their respective joints. The integration of the joints introduces additional mass, resulting in inertia that effectively mitigates spontaneous movements and thereby facilitates smoother motion.

B. Torque Measurements

In this section, we present the results of the torque measurements to evaluate the performance and capabilities of the

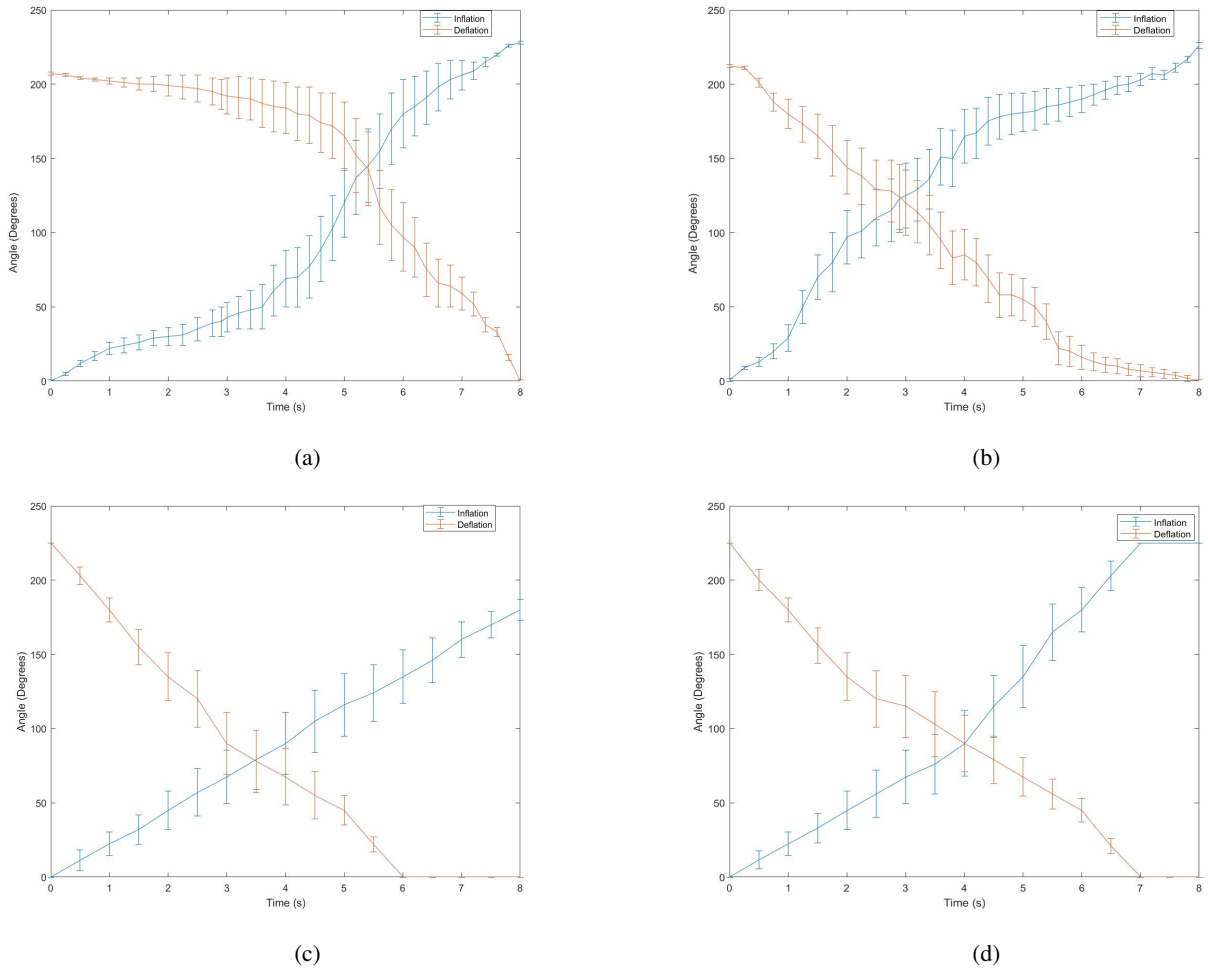

Fig. 10: Performance evaluation of the soft actuators through open-loop tests. Each actuator underwent five inflation and deflation cycles, with measurements captured using a flex sensor. (a) Hinge-style actuator without attachment to a joint. (b) Rotation-style actuator without attachment to a joint. (c) Hinge-style actuator integrated with a joint. (d) Rotation-style actuator integrated with a joint. A total of 40 tests were conducted for a comprehensive assessment.

actuators under different settings. The torque generated by the actuators is a crucial parameter to provide the necessary force for assistance.

The experiments were conducted to measure the torque output of the actuators in different scenarios. Specifically, we investigated the torque of the actuators during hinge joint movements, wide-angle arc motions, and linear inflation.

To measure the torque, a force gauge was employed to capture the applied forces and torques at different joints illustrated in Fig. 7. These measurements were recorded while the actuators operated under controlled conditions. Additionally, the measurements were performed multiple times to ensure the reliability and consistency of the results.

By Analysing the torque characteristics, we can assess the actuators' ability to generate and sustain torque throughout various ranges of motion.

The results of the setup depicted in Fig. 7a are presented in Fig. 11. The torque measured at an angle of 20 degrees was 4.46 Nm, 3 Nm at 40 degrees, 2.59 Nm at 60 degrees, 2.3 Nm at 80 degrees and 1.94 Nm at 100 degrees. Fig. 7b displays a torque of 4.97 Nm at an angle of 45 degrees, but was approximately 5 Nm at all usable angles. Lastly, Fig. 7c displays the maximum force achievable through the actuators by measuring the force linearly, this was measured to be 66.1 N. It is important to note that the exoskeleton does not incorporate a linear joint, and this measurement provides a comprehensive assessment of the force capabilities of the system.

C. Participant experiments to validate assistance

In this experiment, the participant wore the fully integrated device and maintained a relaxed state while the exoskeleton assisted in reaching three targets placed to provide representative movement to each joint in reaching targets in 3-dimensional space. The targets were represented by balls, and the experiment aimed to assess the system's ability to facilitate upper limb motion in reaching these predefined targets within a 3D workspace.

Prior to the experiment, the exoskeleton arm is moved into position and the angles of the joints are recorded to know the

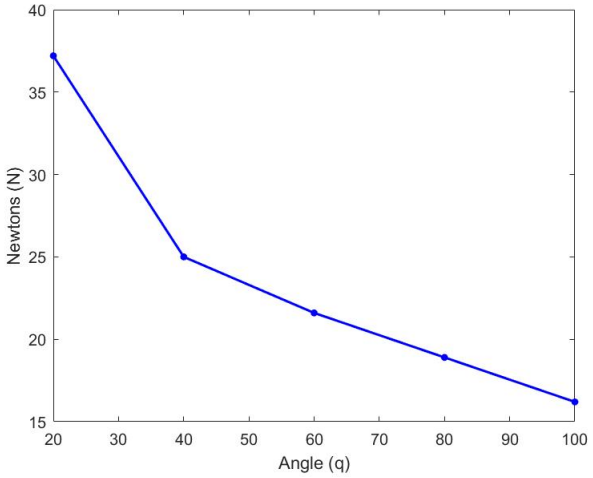

Fig. 11: Relationship between applied force in Newtons and the angle of the hinge actuator. The measurements were obtained by subjecting the hinge actuator to varying angles and measuring the corresponding force exerted at a distance of 0.12 m from the axis of rotation. Due to the precise mechanical setup, the measurements obtained from subjecting the hinge actuator to varying angles and measuring the corresponding force exerted exhibit negligible error.

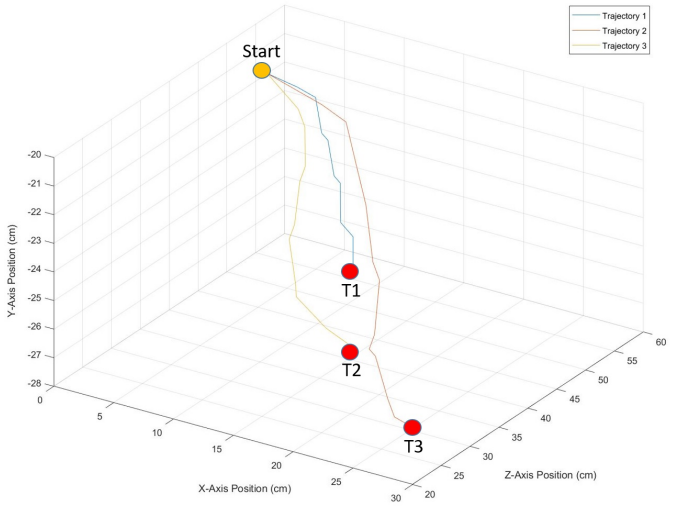

Fig. 12: Trajectories of the three-movement tests depicted relative to the initial position of the end-effector.

final position. The angles throughout are input into the DH model to note the position of the end-effector as depicted in 12.

In the future, the target angles can be determined by a physical therapist while they guide the participant upper limb to decide upon the most suitable motion that the user will benefit from. And the participants can train their motor functions repeatedly as guided by the assistive robots.

To reach each target, five active actuators, along with one passive gravity compensation joint (the shoulder), and one joint without actuators (the spine), were employed in the task reaching experiment.

The movement sequence began with the inflation of the first actuator located at the shoulder. Subsequently, the next actuator in the series was inflated, progressively moving down the arm. This process continued until reaching the last actuator at the wrist. The inflation cycle then restarted from the shoulder, repeating the sequence until all actuators reached their target angles. Each test comprised two inflation cycles, with the total movement of each joint as given by Equation (1) is divided between these two cycles.

The implementation of the incremental inflation approach enabled a straighter trajectory of the end-effector towards the target by reducing deviations. Additionally, this approach allows for individual observation and focus on each joint, offering therapists in a clinical context the ability to modify specific joints and optimise rehabilitation outcomes for targeted areas.

Including more inflation cycles increased erratic motion, possibly attributed to rapid switching between actuators. Conversely, utilising a single cycle resulted in deviations in the movement and increased the time taken to reach the desired position. Simultaneously activating all joints resulted in errors due to the limited capacity of the single pump to distribute pressure adequately throughout the entire arm.

Once the end-effector successfully reached the target, the actuation for the arm was promptly halted. The results of the experiment are depicted in Fig. 12. The recorded time taken to reach each target was as follows: T1 = 9 seconds, T2 = 12 seconds, and T3 = 15.5 seconds.

IV. Discussion

The key findings of the experiment indicated that origami-styled polyethylene actuators can reliably guide and assist users in tasks such as reaching for objects, as shown in Fig. 12. The design of the exoskeleton and spine performed as intended, achieving high manoeuvrability and ultra-lightweight during the experiment. The total weight of the worn device, including 5 soft actuators, the exoskeleton arm, harness, and spine, is 1.8 kg. This weight is more favourable compared to other exoskeletons offering similar functions [9], [15], where the difference in weight is significant. For example, the PLA exoskeleton arm weighs 572 g, while the equivalent in aluminium would be approximately 2.59 kg. Furthermore, the PLA structure can be 3D printed in almost complete form by anyone. The exoskeleton is also mobile, thus, unlike stationary exoskeletons mounted to chairs or beds, there are less constraints on the upper body, and the shoulder position is always aligned with the joints of the exoskeleton.

When compared with 'exosuits' the weight is less favourable and less comfortable to wear, but the weakness of the exosuit is the lack of rigid structure [14], this arguably puts them into a different category of assistive devices. Due to the lack of positioned hard points to actuate from, there is less range of angle rotation in the joints. Additionally, exosuits lack consistent outcomes of reliable repetitive movements i.e. precision.

The soft actuators were developed using an origami style of folding the material over itself in a loop to solve the issue of

leaking, commonly caused by the heat seal connection opening under high pressures [17]. The actuator shape used here has no instances of leaking air during the experiment because they were created using a single tube of folded polyethylene instead of sheets, which reduces the number of heat seals. One of the two heat seals (at the back end) is folded over itself, preventing the internal air pressure from reaching that area. The actuators employed in our study weigh approximately 15 g.

Notably, our actuator design exhibits a favourable force given the size and weight compared to silicone counterparts, as it can generate a torque of 4.46 Nm. In contrast, typically observed silicone actuators produce a maximum torque of approximately 2.7 Nm and are heavier and larger in size [34]. The obtained results demonstrate that these actuators can generate significant torque without breakage, indicating their ability to provide substantial support to the user's arm. This level of torque suggests that the actuators are capable of effectively assisting and augmenting the user's movements.

Also demonstrated is the system's ability to effectively facilitate upper limb motion and reach the predefined targets within the designated 3D workspace. The experiment confirmed the efficacy of the integrated robotic system and highlighted the importance of controlled sequential activation of the soft actuators to achieve accurate and efficient movements towards the targets. Consequently, the physical therapist is able to position the user in performing the repeated motions that involve all joints sequentially to condition the joint motion and establish consistent movement patterns.

Although the actuators exhibited a slower movement compared to the average speed of individuals without physical vulnerabilities, this intentional design choice prioritises safety, as the target users for this medical device are individuals with physical vulnerabilities. Speed can be increased by allowing the actuators to inflate simultaneously instead of sequentially and by increasing the size of the pump, although this would result in increased noise and power requirements.

An important aspect of soft robotics is how to implement impedance control into the user worn device so that the inertia of the device is low enough to not impede user movement. What could potentially be achieved through the utilisation of soft materials is to not only decrease the inertia of human interaction with the device but also passively leverage the extrinsic softness provided by these materials.

Combined with the high degree-of-freedom exoskeleton, this intrinsic softness could prove advantageous in healthcare settings. Individuals with tremors, often associated with Parkinson's disease, could benefit from the external movement reduction provided by the soft modules [35]. Acting as gentle springs, these modules could absorb shaky movements and dampen their impact by counteracting the force from internal pressure and the flexibility of the outer material.

Moreover, a greater application of tensegrity (tensional integrity) principles such as those depicted in the exoskeleton spine could be beneficial in a clinical setting as the elastic stability would function to help vulnerable individuals in a similar way to the soft modules. This approach involves the integration of multiple elastic strips strategically placed over the body, working together to facilitate movement in specific muscles. The elastic materials automatically seek an equilibrium state, thereby reducing the complexity of calculations and enhancing overall system performance.

V. Conclusion

In conclusion, this study presented the development and evaluation of origami-styled polyethylene actuators integrated into an exoskeleton system for upper limb motion assistance. The key findings demonstrate that these actuators can reliably guide and assist users in tasks such as reaching for objects within a 3D workspace. The design of the exoskeleton and spine performed as intended, offering high manoeuvrability and ultra-lightweight characteristics.

Compared to other exoskeletons with similar functions, the weight of the worn device was found to be favourable. This reduced weight contributes to increased comfort and ease of use. Furthermore, the actuator design addressed the issue of leaking air by utilising a single tube of folded polyethylene, minimising the number of heat seals. The absence of air leakage was verified during the experiment, ensuring the actuator's reliability and performance.

The obtained results demonstrated that the actuators generated significant torque without breakage, providing substantial support to the user's arm. This level of torque indicates the effectiveness of the actuators in assisting and augmenting the user's movements. The integrated robotic system effectively facilitated upper limb motion, enabling accurate and efficient reaching of predefined targets.

The study also highlighted the importance of controlled sequential activation of the soft actuators for achieving precise movements towards the targets. While the actuators exhibited somewhat slower movement compared to an average person's speed, this deliberate choice was made for safety purposes, considering the target users with physical vulnerabilities.

Overall, this research demonstrated the potential of origami-styled polyethylene actuators integrated into an exoskeleton system for upper limb assistance. The findings contribute to the advancement of assistive devices for the future of healthcare, offering improved support, manoeuvrability, and reduced weight.

By combining innovative design approaches and soft robotics principles, this study opens up new possibilities for the development of assistive technologies that prioritise user comfort, safety, and precise motion assistance.

Future studies will aim to enhance user control over the device by incorporating sensor technologies. For instance, Electromyography (EMG) can be employed to utilise muscle activity as an input control mechanism. Additionally, incorporating the principles of tensegrity into the exoskeleton offers an innovative approach to its construction and has the potential to enhance its adaptability.

References

[1] Y. Sun and E. P. Zehr, "Training-induced neural plasticity and strength are amplified after stroke," *Exercise and Sport Sciences Reviews*, vol. 47, no. 4, pp. 223–229, Oct. 2019, ISSN: 0091-6331. DOI: 10 . 1249 / JES .

0000000000000199. [Online]. Available: https://www.ncbi.nlm.nih.gov/pmc/articles/PMC6887626/ (visited on 01/13/2021).

[2] V. Gray, C. L. Rice, and S. J. Garland, "Factors that influence muscle weakness following stroke and their clinical implications: A critical review," *Physiotherapy Canada*, vol. 64, no. 4, pp. 415–426, 2012, ISSN: 0300-0508. DOI: 10.3138/ptc.2011-03. [Online]. Available: https://www.ncbi.nlm.nih.gov/pmc/articles/PMC3484914/ (visited on 01/13/2021).

[3] B. R. Brewer, S. K. Mcdowell, and L. C. Worthen-Chaudhari, "Poststroke upper extremity rehabilitation: A review of robotic systems and clinical results," *Topics in Stroke Rehabilitation*, vol. 14, no. 6, pp. 22–44, 2007, ISSN: 1074-9357. DOI: 10.1310/tsr1406-22.

[4] A. C. McConnell, M. Vallejo, R. C. Moioli, *et al.*, "Soft orthotic physiotherapy hand interactive aid," *Frontiers in Mechanical Engineering*, vol. 3, 2017, ISSN: 2297-3079. DOI: 10.3389/fmech.2017.00003. [Online]. Available: https://www.frontiersin.org/articles/10.3389/fmech.2017.00003/full (visited on 10/11/2018).

[5] N. Paredes-Acuna, N. Berberich, E. Dean-Leon, and G. Cheng, "Tactile-based assistive method to support physical therapy routines in a lightweight upper-limb exoskeleton," *IEEE Transactions on Medical Robotics and Bionics*, vol. 4, no. 3, pp. 541–549, 2022, ISSN: 2576-3202. DOI: 10.1109/tmrb.2022.3188429.

[6] N. Jarrassé, T. Proietti, V. Crocher, *et al.*, "Robotic exoskeletons: A perspective for the rehabilitation of arm coordination in stroke patients," *Frontiers in Human Neuroscience*, vol. 8, p. 947, 2014, ISSN: 1662-5161. DOI: 10.3389/fnhum.2014.00947. [Online]. Available: https://www.frontiersin.org/article/10.3389/fnhum.2014.00947.

[7] Younkoo Jeong, Yoon Kyong Kim, Kyunghwan Kim, and Jong-Oh Park, "Design and control of a wearable robot," in *Proceedings 10th IEEE International Workshop on Robot and Human Interactive Communication. ROMAN 2001 (Cat. No.01TH8591)*, 2001, pp. 636–641. DOI: 10.1109/ROMAN.2001.981976.

[8] G. Ma, M. Lin, and Q. Wang, "Mechanical design of a whole-arm exoskeleton rehabilitation robot based on pnf," in *2016 13th International Conference on Ubiquitous Robots and Ambient Intelligence (URAI)*, IEEE. DOI: 10.1109/urai.2016.7733980.

[9] R. C. V. Loureiro, W. S. Harwin, K. Nagai, and M. Johnson, "Advances in upper limb stroke rehabilitation: A technology push," *Medical & Biological Engineering & Computing*, vol. 49, no. 10, pp. 1103–1118, 2011, ISSN: 0140-0118. DOI: 10.1007/s11517-011-0797-0.

[10] A. L. Jutinico, J. C. Jaimes, F. M. Escalante, J. C. Perez-Ibarra, M. H. Terra, and A. A. G. Siqueira, "Impedance control for robotic rehabilitation: A robust markovian approach," *Frontiers in Neurorobotics*, vol. 11, no. 43, 2017, ISSN: 1662-5218. DOI: 10.3389/fnbot.2017.00043. [Online]. Available: https://www.frontiersin.org/article/10.3389/fnbot.2017.00043.

[11] L. Gerez, J. Chen, and M. Liarokapis, "On the development of adaptive, tendon-driven, wearable exo-gloves for grasping capabilities enhancement," *IEEE Robotics and Automation Letters*, vol. 4, no. 2, pp. 422–429, 2019. DOI: 10.1109/LRA.2019.2890853.

[12] H. Al-Fahaam, S. Davis, and S. Nefti-Meziani, "Wrist rehabilitation exoskeleton robot based on pneumatic soft actuators," in *2016 International Conference for Students on Applied Engineering (ICSAE)*, 2016, pp. 491–496. DOI: 10.1109/ICSAE.2016.7810241.

[13] H. Abidi and M. Cianchetti, "On intrinsic safety of soft robots," *Frontiers in Robotics and AI*, vol. 4, 2017, ISSN: 2296-9144. DOI: 10.3389/frobt.2017.00005. [Online]. Available: https://www.frontiersin.org/articles/10.3389/frobt.2017.00005/pdf.

[14] M. Xiloyannis, L. Cappello, K. D. Binh, C. W. Antuvan, and L. Masia, "Preliminary design and control of a soft exosuit for assisting elbow movements and hand grasping in activities of daily living," *Journal of Rehabilitation and Assistive Technologies Engineering*, vol. 4, p. 2055668316680315, 2017, PMID: 31186920. DOI: 10.1177/2055668316680315. eprint: https://doi.org/10.1177/2055668316680315. [Online]. Available: https://doi.org/10.1177/2055668316680315.

[15] C. Carignan, J. Tang, and S. Roderick, "Development of an exoskeleton haptic interface for virtual task training," in *2009 IEEE/RSJ International Conference on Intelligent Robots and Systems*, IEEE. DOI: 10.1109/iros.2009.5354834.

[16] P. Polygerinos, Z. Wang, K. C. Galloway, R. J. Wood, and C. J. Walsh, "Soft robotic glove for combined assistance and at-home rehabilitation," *Robotics and Autonomous Systems*, vol. 73, pp. 135–143, 2015, OA status: gold$_other$, ISSN: 0921-8890. DOI: 10.1016/j.robot.2014.08.014. [Online]. Available: https://manuscript.elsevier.com/S0921889014001729/pdf/S0921889014001729.pdf.

[17] V. W. Oguntosin, Y. Mori, H. Kim, S. J. Nasuto, S. Kawamura, and Y. Hayashi, "Design and validation of exoskeleton actuated by soft modules toward neurorehabilitation—vision-based control for precise reaching motion of upper limb," *Frontiers in Neuroscience*, vol. 11, p. 352, 2017, ISSN: 1662-453X. DOI: 10.3389/fnins.2017.00352. [Online]. Available: https://www.frontiersin.org/article/10.3389/fnins.2017.00352.

[18] B. R. Brewer, S. K. McDowell, and L. C. Worthen-Chaudhari, "Poststroke upper extremity rehabilitation: A review of robotic systems and clinical results," *Top Stroke Rehabil*, vol. 14, no. 6, pp. 22–44, 2007, Brewer, Bambi R McDowell, Sharon K Worthen-Chaudhari, Lise C eng Review England 2008/01/05 Top Stroke Rehabil. 2007 Nov-Dec;14(6):22-44. doi: 10.1310/tsr1406-22., ISSN: 1074-9357 (Print) 1074-9357 (Linking). DOI: 10.1310/tsr1406-22. [Online]. Available: https://www.ncbi.nlm.nih.gov/pubmed/18174114.

[19] C. D. Takahashi, L. Der-Yeghiaian, V. Le, R. R. Motiwala, and S. C. Cramer, "Robot-based hand motor ther-

apy after stroke," *Brain*, vol. 131, no. 2, pp. 425–437, Dec. 2007, ISSN: 0006-8950. DOI: 10.1093/brain/awm311. eprint: https://academic.oup.com/brain/article-pdf/131/2/425/1133344/awm311.pdf. [Online]. Available: https://doi.org/10.1093/brain/awm311.

[20] X. Li, Y. Pan, G. Chen, and H. Yu, "Adaptive human–robot interaction control for robots driven by series elastic actuators," *IEEE Transactions on Robotics*, vol. 33, no. 1, pp. 169–182, 2017, ISSN: 1552-3098. DOI: 10.1109/tro.2016.2626479.

[21] H. Al-Fahaam, S. Davis, and S. Nefti-Meziani, "Wrist rehabilitation exoskeleton robot based on pneumatic soft actuators," in *2016 International Conference for Students on Applied Engineering (ISCAE)*, IEEE. DOI: 10.1109/icsae.2016.7810241.

[22] A. Calanca, L. Capisani, and P. Fiorini, "Robust force control of series elastic actuators," *Actuators*, vol. 3, no. 3, pp. 182–204, 2014, ISSN: 2076-0825. DOI: 10.3390/act3030182. [Online]. Available: https://dx.doi.org/10.3390/act3030182.

[23] J. Li, H. Godaba, Z. Zhang, C. Foo, and J. Zhu, "A soft active origami robot," *Extreme Mechanics Letters*, vol. 24, pp. 30–37, 2018, ISSN: 2352-4316. DOI: 10.1016/j.eml.2018.08.004.

[24] S. A. Zirbel, "Compliant mechanisms for deployable space systems," vol. 5612, 2014-11-01. DOI: http://hdl.lib.byu.edu/1877/etd7321. [Online]. Available: https://scholarsarchive.byu.edu/cgi/viewcontent.cgi?article=6611%5C&context=etd.

[25] B. Jasim and P. Taheri, "An origami-based portable solar panel system," in *2018 IEEE 9th Annual Information Technology, Electronics and Mobile Communication Conference (IEMCON)*, IEEE. DOI: 10.1109/iemcon.2018.8614997.

[26] C. D. Onal, M. T. Tolley, R. J. Wood, and D. Rus, "Origami-inspired printed robots," *IEEE/ASME Transactions on Mechatronics*, vol. 20, no. 5, pp. 2214–2221, 2015, ISSN: 1083-4435. DOI: 10.1109/tmech.2014.2369854.

[27] Z. Kan, Y. Zhang, Y. Yang, Y. A. Tse, and M. Y. Wang, "An origami-inspired monolithic soft gripper based on geometric design method," in *2019 2nd IEEE International Conference on Soft Robotics (RoboSoft)*, IEEE. DOI: 10.1109/robosoft.2019.8722746.

[28] W. H. Chang and Y.-H. Kim, "Robot-assisted therapy in stroke rehabilitation," *Journal of Stroke*, vol. 15, no. 3, p. 174, 2013, ISSN: 2287-6391. DOI: 10.5853/jos.2013.15.3.174. [Online]. Available: https://dx.doi.org/10.5853/jos.2013.15.3.174.

[29] S. Kousidou, N. Tsagarakis, D. Caldwell, and C. Smith, "Assistive exoskeleton for task based physiotherapy in 3-dimensional space." DOI: 10.1109/biorob.2006.1639097.

[30] D. Buongiorno, E. Sotgiu, D. Leonardis, S. Marcheschi, M. Solazzi, and A. Frisoli, "Wres: A novel 3 dof wrist exoskeleton with tendon-driven differential transmission for neuro-rehabilitation and teleoperation," *IEEE Robotics and Automation Letters*, vol. 3, no. 3, pp. 2152–2159, 2018, ISSN: 2377-3766. DOI: 10.1109/lra.2018.2810943.

[31] J. Ma, D. Chen, Z. Liu, and M. Wang, "A soft wearable exoskeleton with pneumatic actuator for assisting upper limb," 2020. DOI: 10.1109/rcar49640.2020.9303269.

[32] M. F. Ashby, *Materials Selection in Mechanical Design*, 4th. Oxford, UK: Butterworth-Heinemann, 2011.

[33] K. Caluwaerts, J. Despraz, A. Işçen, *et al.*, "Design and control of compliant tensegrity robots through simulation and hardware validation," *Journal of The Royal Society Interface*, vol. 11, no. 98, p. 20 140 520, 2014, ISSN: 1742-5689. DOI: 10.1098/rsif.2014.0520. [Online]. Available: https://dx.doi.org/10.1098/rsif.2014.0520.

[34] V. Oguntosin, W. S. Harwin, S. Kawamura, S. J. Nasuto, and Y. Hayashi, "Development of a wearable assistive soft robotic device for elbow rehabilitation," in *2015 IEEE International Conference on Rehabilitation Robotics (ICORR)*, 2015, pp. 747–752. DOI: 10.1109/ICORR.2015.7281291.

[35] A. Zahedi, B. Zhang, A. Yi, and D. Zhang, "A soft exoskeleton for tremor suppression equipped with flexible semiactive actuator," *Soft Robotics*, vol. 8, Aug. 2020. DOI: 10.1089/soro.2019.0194.

Daniel George received his BSc and MEng degree in Cybernetics at the University of Reading, UK in 2018. He is currently pursuing a PhD in Biomedical Engineering from the University of Reading. His scientific activity focuses on soft-actuated lightweight exoskeletons for movement assistance.

Sadao Kawamura received the B.S. degree in biophysical engineering, the M.S. degree in mechanical engineering, and the Ph.D. degree in mechanical engineering from Osaka University, Osaka, Japan, in 1981, 1983, and 1986, respectively. He was an Assistant Professor with Osaka University from 1986 to 1987, and an Associate Professor with Ritsumeikan University, Kyoto, Japan, from 1987 to 1994. Since 1996, he has been a Professor in the Department of Robotics, Ritsumeikan University. Since 2011, he has been the Director of Advanced Research Center of Robotics, Ritsumeikan University. From 2003 to 2006, he was a Vice President of Ritsumeikan University. Dr. Kawamura received SICE Best Paper Award in 1987, 2000, and 2009, the ISCIE Best Paper Award in 1987, the Fluid Power Technology Promotion Foundation Best Paper Award in 1992 and 2010, and the Good Design Special Award in 2001. He is an Associate Member of the Science Council of Japan, a Member of the Engineering Academy of Japan, and a Fellow of Japan Society of Mechanical Engineering. From 2011 to 2013, he was the President of the Robotics Society of Japan.

Ying Zheng received her BEng and PhD from the University of Sheffield, UK. She is currently a Professor at the University of Reading in the Department of Biological Sciences. She has been working in the interface of systems engineering and neuroscience for over 10 years. The main direction of her research is to develop mathematical models to understand neural and haemodynamic signals obtained from neuroimaging techniques such as microelectrodes, EEG, laser-Doppler flowmetry, optical imaging spectroscopy and fMRI.

Yoshikatsu Hayashi received a BSc in Cell biology from University of Tokyo, Japan and a PhD in Statistical physics of soft matter from Lund University, Sweden in 2004. He is currently an Associate Professor at the University of Reading in the Department of Biological Sciences. He is interested in neuroscience, behavioural science and physics in complex systems; revealing 1) Nonlinear dynamics governing adaptation behaviour in living creatures, 2) Closed loop of brain and body (neural networks and sensory-motor systems), and 3) Mathematical structure underlying behaviour and neural networks.